International Journal of Innovative
Computing, Information and Control
Volume **8**, Number **1(B)**, January **2012**

 ISSN 1349-4198
pp. 527–538

ULTRASONIC TOMOGRAPHY – IMAGE RECONSTRUCTION ALGORITHMS

Mohd Hafiz Fazalul Rahiman[1], Ruzairi Abdul Rahim[2]
Herlina Abdul Rahim[2], Siti Zarina Mohd Muji[3]
and Elmy Johana Mohamad[3]

[1]School of Mechatronic Engineering
Universiti Malaysia Perlis
Ulu Pauh Campus, 02600 Arau, Perlis, Malaysia
hafiz@unimap.edu.my

[2]Faculty of Electrical Engineering
Universiti Teknologi Malaysia
81310 UTM Skudai, Johor, Malaysia
{ ruzairi; herlina }@fke.utm.my

[3]Faculty of Electrical and Electronic Engineering
Universiti Tun Hussein Onn Malaysia
86400 Parit Raja, Batu Pahat, Johor, Malaysia
{ szarina; elmy }@uthm.edu.my

Received August 2010; revised December 2010

Abstract. *This paper focuses on image reconstruction algorithms for use in ultrasonic tomography. There are three types of algorithms namely Linear Back Projection, Hybrid Reconstruction and Hybrid Binary Reconstruction that are of interest. The algorithms have been evaluated on ultrasonic tomography system based on several known phantoms and real objects. The performance of the algorithms have been analyzed and discussed at the end of the paper. A recommendation of suitable reconstruction algorithm for liquid/gas flows has also been made at the end of the paper.*
Keywords: Reconstruction algorithm, Ultrasonic tomography, Image processing

1. **Introduction.** Most of tomographic images were derived from back projection algorithm. In order to derive this algorithm which results in the solution to the inverse problem, the forward problem must be solved first.

The forward problem determines the theoretical output of each of the sensors when the sensing area is considered to be two-dimensional. The forward problem can be solved by using the analytical solution of sensitivity maps which produces the sensitivity matrices [1]. The sensitivity distribution can be determined by calculating the ultrasonic energy attenuation at position of each receiver due to obstruction in the object space.

The inverse problem is then to determine from the system response matrix (sensitivity matrices), a complex transformation matrix for converting the measured sensor values into pixel values that is the tomogram.

Most of the work in process tomography has focused on the back projection technique. It is originally developed for the X-ray tomography and it also has the advantages of low computation cost [2]. The measurements obtained at each projected data are the attenuated sensor values due to object space in the image plane. These sensor values are then back projected by multiplying with the corresponding normalized sensitivity maps [3]. The back projected data values are smeared back across the unknown density function

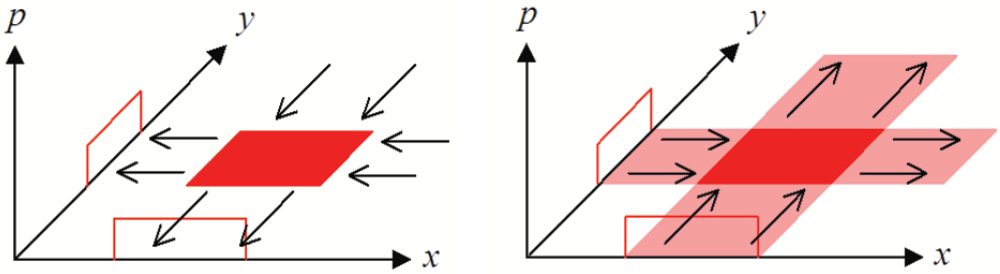

(a) Projection (b) Back projection

FIGURE 1. The back projection method

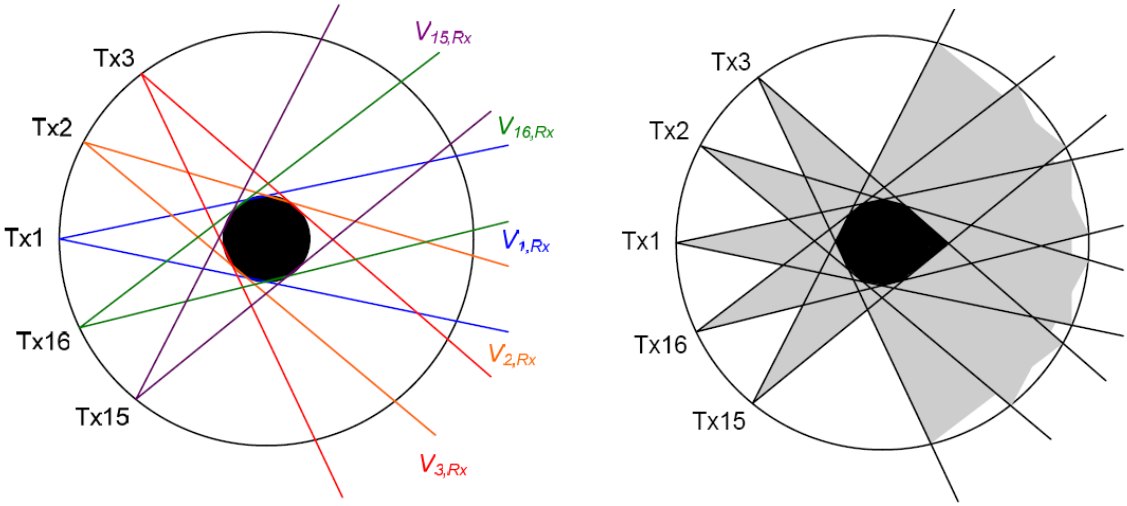

(a) Projection (b) Back projection

FIGURE 2. The fan-shaped beam back projection

(image) and overlapped to each other to increase the projection data density. The process of back projection is shown in Figures 1 and 2.

The density of each point in the reconstructed image is obtained by summing up the densities of all rays which pass through that particular point [4]. This process may be described by Equation (1). Equation (1) is the back projection algorithm where the spoke pattern represents blurring of the object in space.

$$f_b(x,y) = \sum_{j=1}^{m} g_j(x\cos\theta_j + y\sin\theta_j)\Delta\theta \tag{1}$$

where $f_b(x,y)$ = the function of reconstructed image from back projection algorithm, θ_j = the j-th projection angle and $\Delta\theta$ = the angular distance between projection and the summation extends over all the m projection.

Ultrasonic flow imaging systems require quite different reconstruction algorithms because of the form in which the measured data are obtained. Essentially, it is due to a set of time delay measurements that gives the distance of object media interfaces from the receiving sensors [3]. Besides, the ultrasound propagation depends on the medium, which

in this case focuses on liquid/gas medium. The uncertain liquid condition such as wavy may also lead to the uncertain sensor values and as well as the reconstructed images.

2. **Linear Back Projection Algorithm.** In Linear Back Projection algorithm (LBP), the concentration profile is generated by combining the projection data from each sensor with its computed sensitivity maps [5]. The modeled sensitivity matrices are used to represent the image plane for each view. To reconstruct the image, each sensitivity matrix is multiplied by its corresponding sensor loss value; this is the same as back project each sensor loss value to the image plane individually [3]. Then, the same elements in these matrices are summed to provide the back projected voltage distributions (concentration profile) and finally these voltage distributions will be represented by the color level (colored pixels) [6]. This process can be expressed mathematically as below [3]:

$$V_{LBP}(x,y) = \sum_{Tx=1}^{m} \sum_{Rx=1}^{n} S_{Tx,Rx} \times \overline{M}_{Tx,Rx}(x,y) \tag{2}$$

where $V_{LBP}(x,y)$ = voltage distribution obtained using LBP algorithm in the concentration profile matrix and $S_{Tx,Rx}$ = sensor loss voltage for the corresponding transmission (Tx) and reception (Rx).

3. **Hybrid Reconstruction Algorithm.** The Hybrid Reconstruction algorithm (HR) is based on the previous development by Ibrahim [7]. This algorithm determines the condition of projection data and improves the reconstruction by marking the empty area during image reconstruction. As a result, the smearing effect caused by the back projection technique is reduced. The projection data obtained by Ibrahim [7] is based on the sensor value. Later, Chan [8] had used a different approach where he used the signal loss measurement instead of direct projection data in order to reconstruct the fan-shaped beam image through optical technique. He claimed that this method is easier to implement compared with the original method. The HR is obtained by multiplying the concentration profile obtained using the LBP with the HR masking matrix.

The HR masking matrix was obtained by filtering each of the concentration profile element. If the concentration profile element is larger or equal to 3/4 of the maximum pixel value, then the masking matrix element for the corresponding concentration profile element is set to one otherwise it is set to zero. The mathematical model for HR is shown as below:

$$V_{HR}(x,y) = B_{HR}(x,y) \times V_{LBP}(x,y) \tag{3}$$

in which:

$$\begin{aligned} B_{HR}(x,y) = 0 &\Rightarrow V_{LBP}(x,y) < P_{Th} \\ B_{HR}(x,y) = 1 &\Rightarrow V_{LBP}(x,y) \geq P_{Th} \end{aligned} \tag{4}$$

where $B_{HR}(x,y)$ = HR masking matrix, P_{Th} = pixel threshold value (3/4 of the maximum value), $V_{LBP}(x,y)$ = reconstructed concentration profile using LBP and $V_{HR}(x,y)$ = improved concentration profile using HR.

4. **Hybrid Binary Reconstruction Algorithm.** For comparison with the LBP and HR method, another image reconstruction technique has been employed namely the Hybrid Binary Reconstruction algorithm (HBR). This algorithm has the advantage of improving the stability and repeatability of the reconstructed image. The HBR is obtained by multiplying each sensor value to its corresponding sensitivity map. If the sensor value is higher or equal to the threshold voltage, (V_{Th}) then its projection path which is represented by the sensitivity map is set to a maximum pixel value (i.e., 511), otherwise it is set to a minimum pixel value (i.e., 0).

If along the projection path consist of discontinuous component (gas), the transmitted ultrasound energy will be totally reflected and thus no ultrasound signal detected at the receiver. Therefore, a threshold voltage must be first selected. This threshold voltage is needed for the purpose of separating the object from the background, thus creating a binary picture from a picture data (tomogram). This procedure is only appropriate for two-phase flow imaging in cases where the phases are well separated such as liquid-gas flow [9].

Besides, the dynamic characteristic of liquid-gas flow is most probably uncertain and it is quite hard to predict the behavior of such flow. For industrial flow, the sudden changes in term of pressure lead to wavy flow. This may result the sensor value to fluctuate randomly and causes to the unknown image reconstructed as well as increases the measurement error. By thresholding the sensor value, it limits the sensor value fluctuation and therefore minimizes the measurement error. The mathematical model for HBR is shown as follows:

$$V_{HBR}(x,y) = \sum_{Tx=1}^{m} \sum_{Rx=1}^{n} V_{Tx,Rx} \times \overline{M}_{Tx,Rx}(x,y) \tag{5}$$

in which

$$\begin{array}{ll} V_{HBR}(x,y) = 0 & \Rightarrow V_{Tx,Rx} < VTh \\ V_{HBR}(x,y) = 511 & \Rightarrow V_{Tx,Rx} \geq VTh \end{array} \tag{6}$$

where $V_{Tx,Rx}$ = the sensor value and $V_{HBR}(x,y)$ = concentration profile obtained using HBR. The reconstruction method is represented in the flow chart in Figure 3.

5. **Image Area and Error Measurement.** The quality of a tomographic flow imaging system can be judged by comparing the reconstructed image of a physical model with the actual cross-section [9,10]. The comparison is performed on the image reconstruction computer against a standard image (test model) which matches the cross-section of the physical model. The image plane representing the cross-section of the experimental column is divided into M square image pixels. A 64×64 array pixels image has been chosen for displaying the reconstructed image. Thus, $M = 3320$ pixels where another 776 pixels lie outside the column boundary. Ideally, the reconstructed image should be identical to the standard image (the test model), but in practice differences arise.

The liquid and gas distribution in the tomogram are calculated using the following equation:

$$AG = \left(\frac{\sum_{y=1}^{64} \sum_{x=1}^{64} V(x,y)}{M_p} \right) \times 100\% \tag{7}$$

$$AL = \left(1 - \frac{\sum_{y=1}^{64} \sum_{x=1}^{64} V(x,y)}{M_p} \right) \times 100\% \tag{8}$$

where A_G = the gas area percentage, A_L = the liquid area percentage, $V(x,y)$ = the obtained pixel values for 64×64 pixels concentration profile and M_p = the total pixels value that is 1696520.

The gas area percentage is obtained by summing each of the pixel values in the concentration profile matrix and divide with the total pixels value. A 64×64 square matrix has a number of 4096 pixels but only 3320 pixels contribute to represent the image plane and

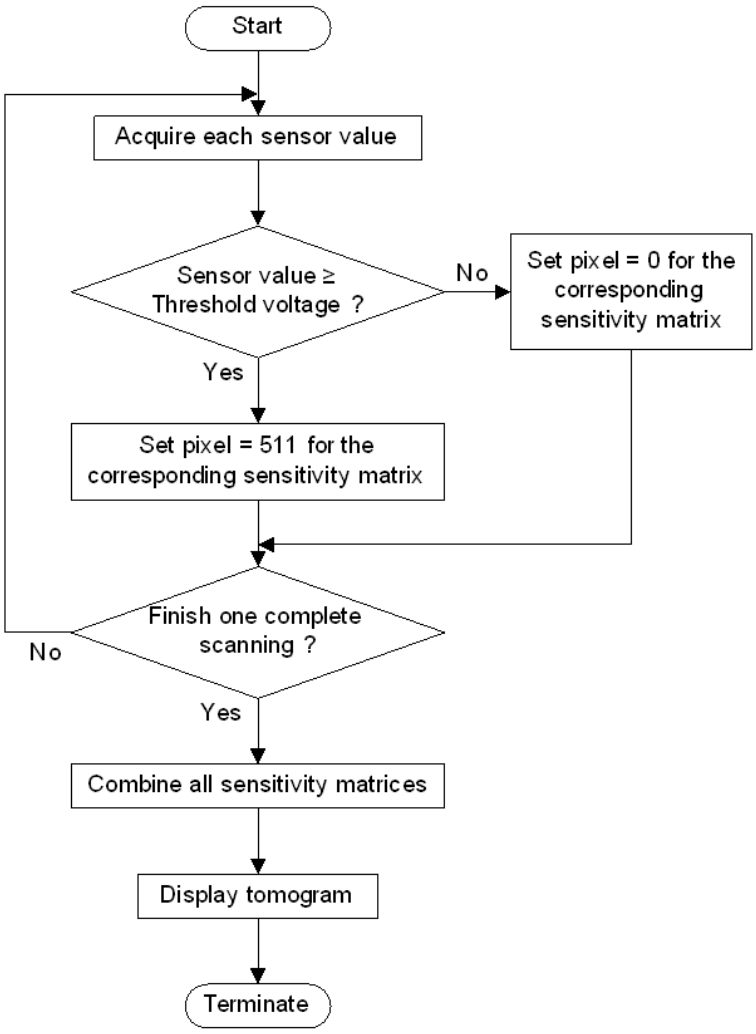

FIGURE 3. The HBR flowchart

another 776 pixels lie outside the column boundary. Each pixel has a maximum value of 511 and therefore, the total pixels value are obtained by multiply the 3320 pixels with the maximum pixel value that is 511 and resulting 1696520. Meanwhile, the liquid area percentage is obtained by simply deducing the normalized gas area by one.

The error information, however, can be obtained using the area error, AE which is defined as below [11].

The standard image in Figure 4 is an array of M pixels defining the standard (test) model by the colour level of each pixel:

$$GS(p) = \begin{cases} 0 & \text{for pixels occupied by Gas component } (\varepsilon_1) \\ GM & \text{for pixels occupied by Liquid component } (\varepsilon_2) \end{cases} \tag{9}$$

$$GB(p) = \begin{cases} 0 & G_R(p) = 0 \\ GM & G_R(p) > 0 \end{cases} \quad (p = 1, 2, \ldots, M) \tag{10}$$

in which:

$$AE = \frac{\sum_{p=1}^{M} G_B(p) - \sum_{p=1}^{M} G_S(p)}{\sum_{p=1}^{M} G_S(p)} = \frac{N_R - N_S}{N_S} = \frac{N_R}{N_S} - 1 \tag{11}$$

where $G_S(p)$ = the standard (test) model pixels, $G_M(p)$ = the colour level assigned to the liquid component, $G_B(p)$ = the binary reconstructed image pixels, N_R = the number of pixels with non-zero colour levels in the reconstructed images and N_S = the number of pixels with non-zero colour levels in the standard images.

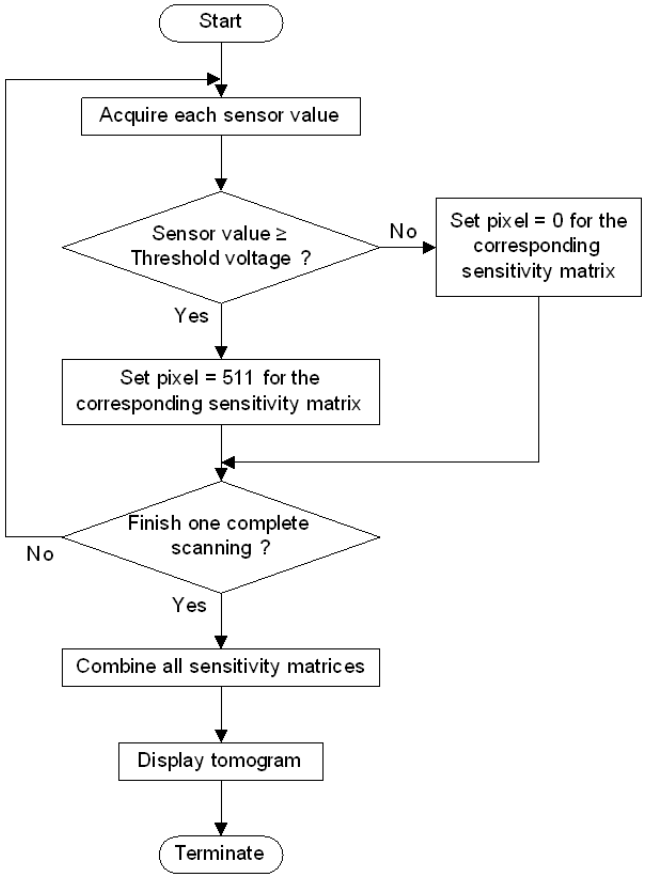

FIGURE 4. Image reconstruction error measurement models

However, AE value is preferably presented in percentages by multiplying with 100%. The value of AE that negative indicates that the reconstructed object is always smaller than the standard models whereas the positive value of AE indicates the reconstructed object is always larger compared to the standard models.

6. **Results.** In this section, results for the reconstruction algorithm simulations of several test profiles and the real-time reconstructed image for several experiments are presented and discussed. The experiments involve simulation from the forward models and real-time measurement on the test profiles for stratified and annular flows.

6.1. **The stratified flows.** Stratified flow regime is created by placing the experimental column horizontally such that the gas phase (air) flows in the upper section of the column and the liquid (water) in the lower section. Horizontal column with static liquid model was used to simulate the stratified flow.

The liquid component was determined based on Equation (8) using all three reconstruction algorithms from 10% flow to 100% flow with increment of 5% for each real-time measurement taken. The standard model samples are based on mathematical calculation of liquid areas. Figure 5 shows the liquid area percentages against the standard model for stratified flows.

The *Area Error* (AE) has been calculated for the real-time measurement made using LBP, HR and HBR in the stratified flows based on Equation (11) and it is shown in Figure 6. The tomogram images for three quarter flow of forward model and real-time measurement are shown in Figure 7.

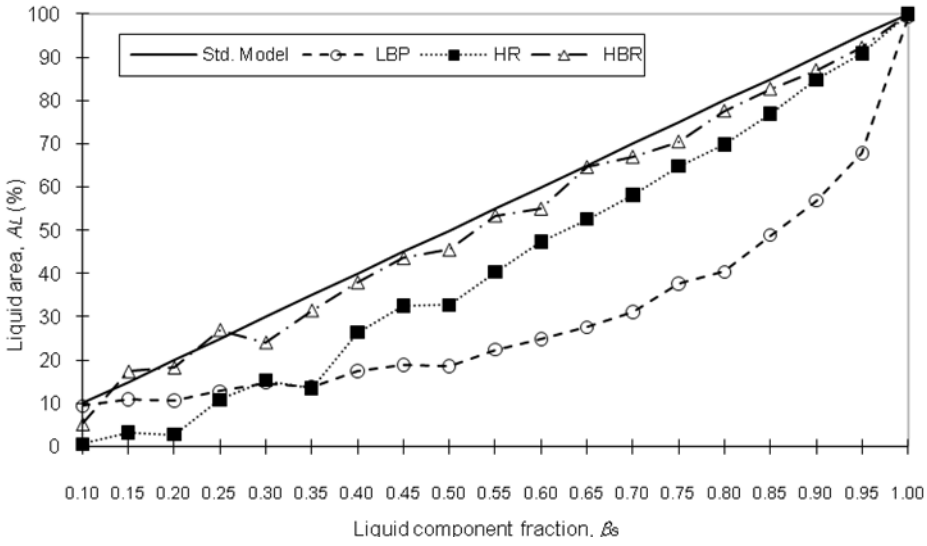

FIGURE 5. The liquid area for stratified flow

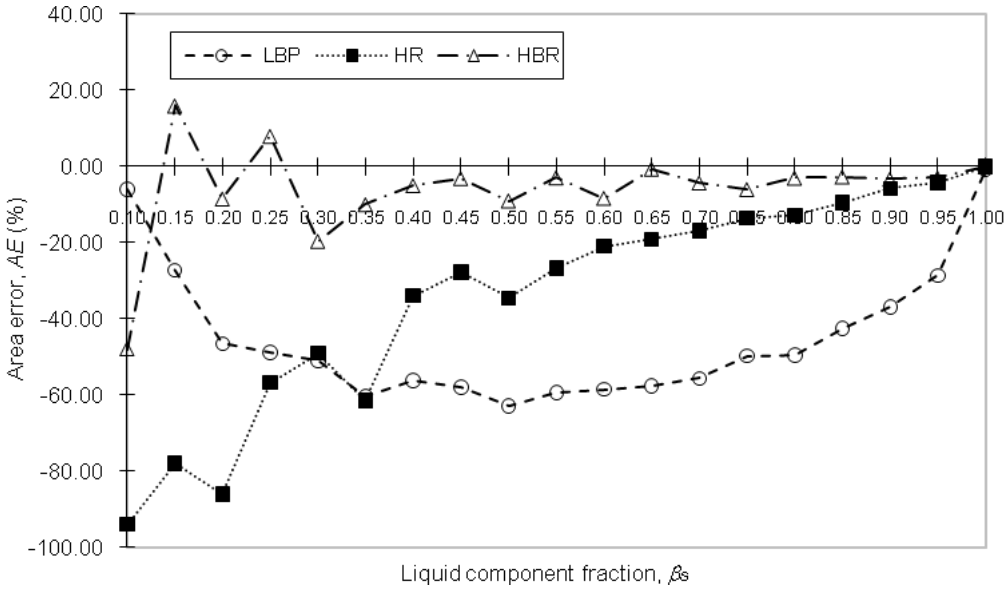

FIGURE 6. AE for the stratified flow

In stratified flow, the reconstructed images by LBP seem to produce much smearing effects. Meanwhile, the *Area Error* (AE) was found highest during the half flow that is -62.8% and the lowest value during full liquid flow that is -0.7%. On the other hand, the reconstructed images by HR are more likely affected by these smearing effects. As shown in Figure 7, the smearing effects mostly contributed by high pixel values. Thus, the threshold in the HR seems unable to reduce this false image.

Compared with LBP and HR, the HBR had removed these false images completely. The image reconstructed by HBR mostly preserved their shapes and positions and therefore the stratified flow regime can be clearly identified. However, the HBR is not superior

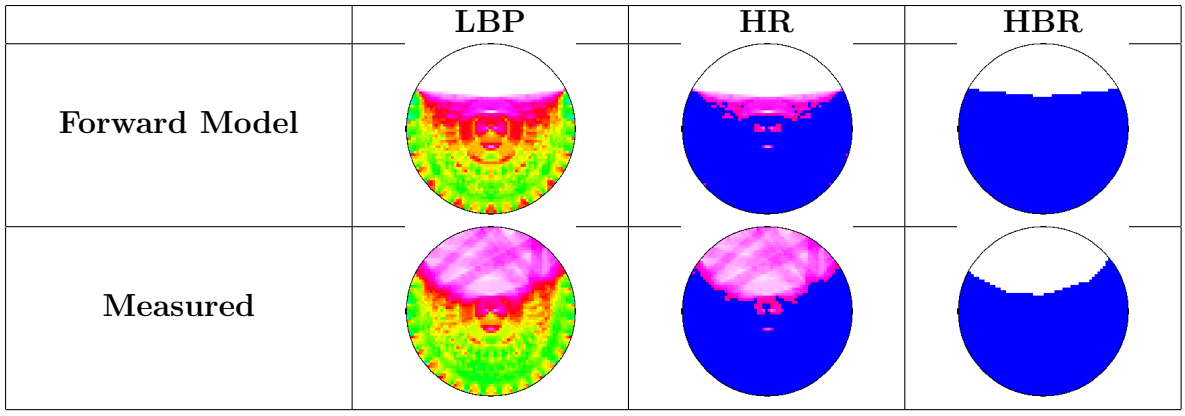

FIGURE 7. The tomogram for three quarter flow of forward model and real-time measurement

during low liquid flow especially at $\beta_s = 0.1$ which has *Area Error* at -48%. It is because during low liquid flow, most of the column section is occupied by the gas component which provide high acoustic impedance region. Thus, the number of measurement has been limited to low acoustic impedance in the liquid segment. The *Area Error* in HBR reconstruction however tends to improve as the liquid component fraction increases.

6.2. **The annular flows.** Annular flow regime is obtained when an empty circular tube (gas model) was inserted in the centre of the column and the gap between the tube and column was filled with liquid (water). Several test models with different diameter was used to simulate multi–diameter annular flow regime. The annular flow model diameter, A_d are 21.6mm, 27.0mm, 33.7mm, 42.2mm, 48.6mm, 60.5mm and 82.8mm. Using the same approach, the liquid area percentages and the *Area Error* for annular flow is calculated and shown in Figures 8 and 9 respectively. The tomogram images for annular flow of forward model and real-time measurement are shown in Figure 10.

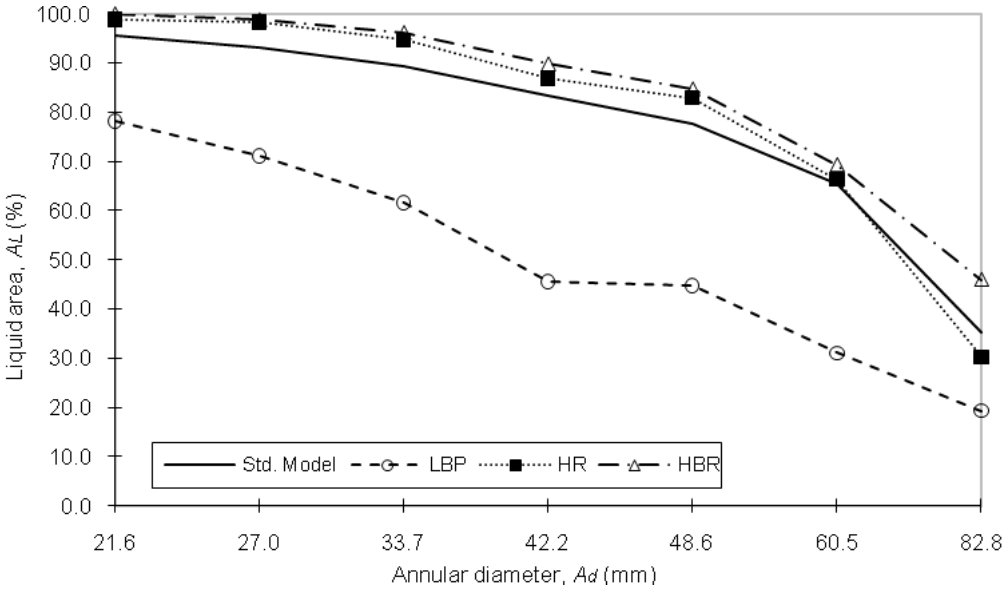

FIGURE 8. The liquid area for annular flow

In annular flow, the reconstructed images by LBP and HR have not much affected by the smearing effects of back projection technique. In this case, the reconstructed image clearly indicates the annular flow segment. In addition, the shape and position of annular

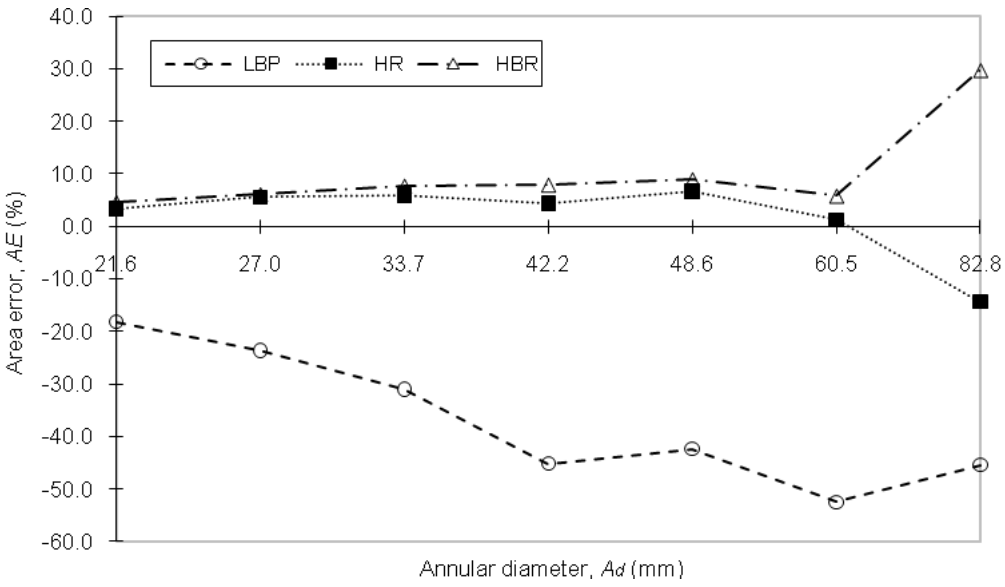

FIGURE 9. *AE* for the annular flow

flow which consist of liquid/gas component is more a less the same with the simulated flow regime. From Figure 9, it is found that the *Area Error* increases as the annular flow diameter increases. This is because the false image which filled within the gas section contributes to the error statistics.

From the observations, it is found that the *Area Error* by HR and HBR technique are almost constant. For HBR, it showed that the reconstructed images are always larger than the test model. This phenomena is because, HBR reconstruct image using the sensor value. Thus, the reconstructed image depends on the sensor's resolution and also the number of measurements taken.

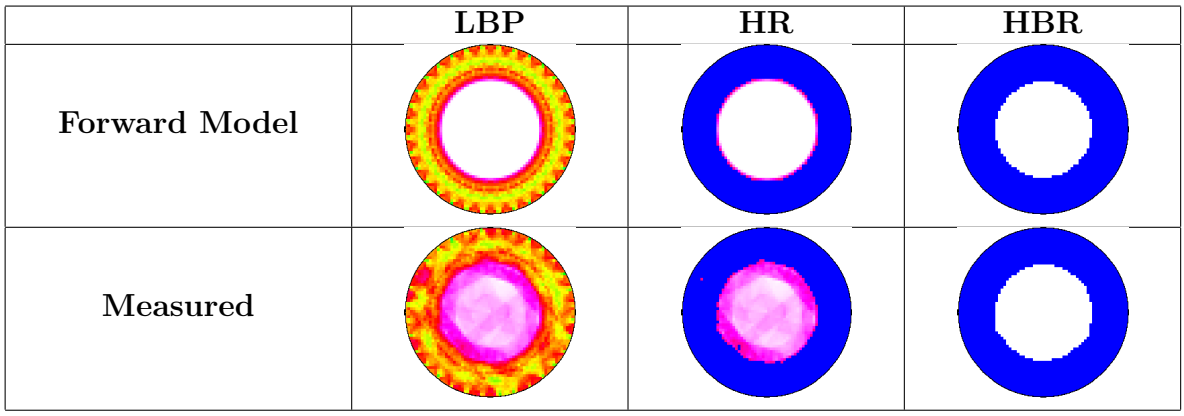

FIGURE 10. The tomogram for annular flow of forward model and real-time measurement

6.3. **The slug flows.** The cross-section image of a slug flow was created by an empty circular tube (gas model) is placed near to the pipe wall and the gap between the tube and pipe was filled with liquid (water). The slug flow experiment was carried out for three different gas model diameters that are 42.2mm diameter, 48.6mm diameter and 60.5mm diameter. The liquid area percentages and the *AE* obtained from the slug flow are shown in Figure 11 and Figure 12 respectively. The tomogram images for slug flow obtained from real-time measurement are shown in Figure 13.

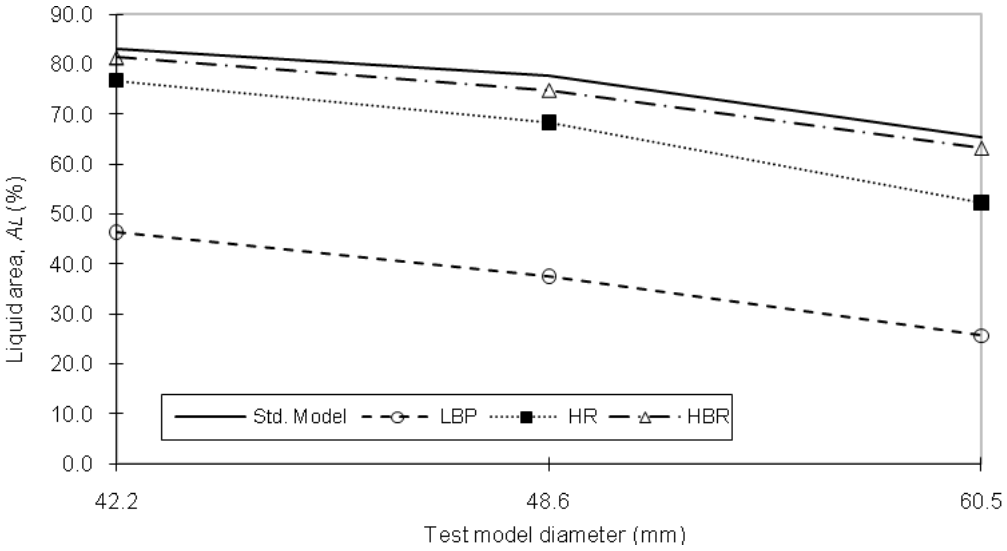

FIGURE 11. The liquid area for slug flow

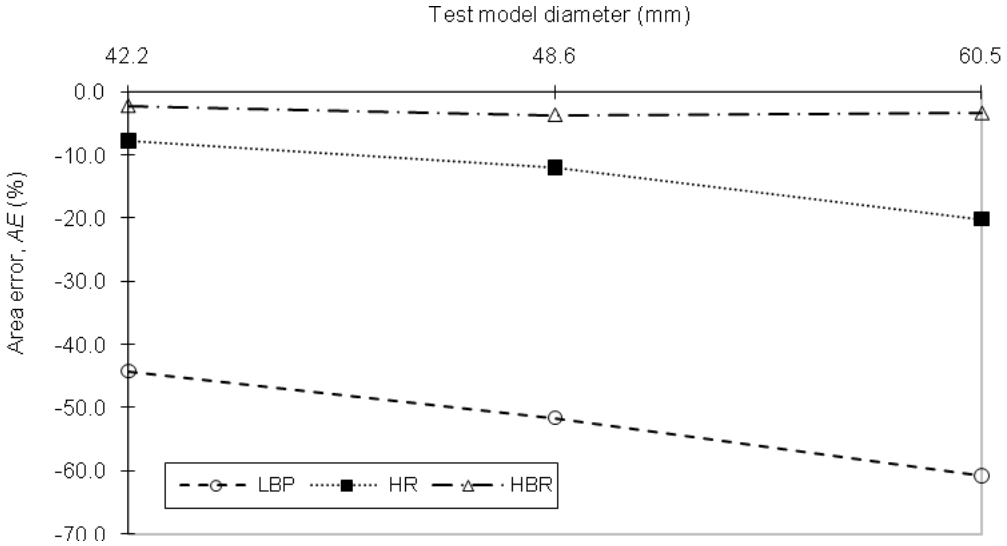

FIGURE 12. *AE* for slug flow

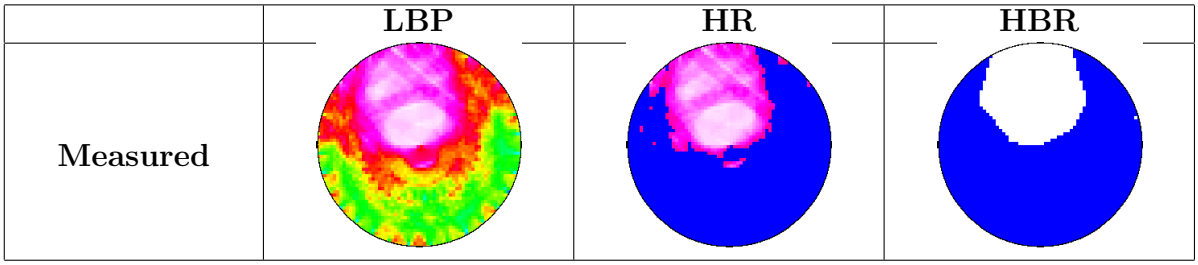

FIGURE 13. The slug flow with 48.6mm model diameter

As seen from the reconstructed image, the drawback of the LBP is that the algorithm smears out between liquid and gas interfaces. This drawback had affected the concentration measurement and therefore leads to the highest *Area Error* statistics and this is shown in Figure 12. However, the overall reconstruction shows acceptable slug flow pattern.

Although the HR method could improve the blurry image, but for poorly reconstructed slug flow in Figure 13, the HR method fails to improve the reconstruction. Most of the problem with HR method is that, the threshold only filter low pixel value, hence the blurry image that caused by high pixel value will be sustained. Compared with HBR technique, the digitized sensor value had removed the false image completely. Moreover, the shape and position of slug flow in the reconstructed image had clearly identified. As a result, the *Area Error* of HBR as in Figure 12 had shown the minimum for all three cases.

7. **Conclusions.** This paper presents three types of image reconstruction algorithm namely the Linear Back Projection (LBP), Hybrid Reconstruction (HR) and Hybrid Binary Reconstruction (HBR). Three types of flow regime namely three quarter, annular and slug flow have been tested using these algorithms. The results showed that, the image reconstructed by LBP results in blurring the image which leads to high AE in every measurement taken. This blurring image is due to the nature of back-projection technique. However, the blurring image was reduced by using HR algorithm but smearing effects of high pixel value is still obvious. Implementing the HBR algorithm had eliminated all the smearing effects and resulting lowest *Area Errors* in overall reconstructions. Thus, the HBR has become the most suitable reconstruction algorithm for liquid and gas flow compared to LBP and HR algorithms.

Acknowledgment. This work is partially supported by Ministry of Higher Education Malaysia, Universiti Malaysia Perlis and Universiti Teknologi Malaysia (GUP vot. no. H01). The authors also gratefully acknowledge the helpful comments and suggestions of the reviewers, which have improved the presentation of the manuscript.

REFERENCES

[1] D. Miyazaki, K. Ito, Y. Nakao, T. Toyoda and Y. Masaki, Reconstruction of three-dimensional image from compound-eye imaging with defocus using ray tracing, *International Journal of Innovative Computing, Information and Control*, vol.5, no.11(B), pp.4225-4235, 2009.

[2] C. A. Garcia-Stewart, N. Polydorides, K. B. Ozanyan and H. McCann, Image reconstruction algorithms for high-speed chemical species tomography, *Proc. of the 3rd World Congress on Industrial Process Tomography*, Banff, Canada, pp.80-85, 2003.

[3] M. H. Fazalul Rahiman, R. Abdul Rahim and M. Tajjudin, Ultrasonic transmission-mode tomography imaging for liquid/gas two-phase flow, *IEEE Sensors J.*, vol.6, no.6, pp.1706-1715, 2006.

[4] R. Sammouda, J. A. Hassan and M. Sammouda, CT image analysis for early detection of lung cancer, *International Journal of Innovative Computing, Information and Control*, vol.4, no.11, pp.2847-2860, 2008.

[5] R. Abdul Rahim, M. H. Fazalul Rahiman, K. S. Chan and S. W. Nawawi, Non-invasive imaging of liquid/gas flow using ultrasonic transmission-mode tomography, *Sensors and Actuators A*, vol.135, no.2, pp.337-345, 2007.

[6] T. R. McKeen and T. S. Pugsley, The influence of permittivity models on phantom images obtained from electrical capacitance tomography, *Measurement Science Technology*, vol.13, no.12, pp.1822-1830, 2002.

[7] S. Ibrahim, *Measurement of Gas Bubbles in a Vertical Water Column Using Optical Tomography*, Ph.D. Thesis, Sheffield Hallam University, 2000.

[8] K. S. Chan, *Real-Time Image Reconstruction for Fan Beam Optical Tomography System*, Master Thesis, Universiti Teknologi Malaysia, 2002.

[9] A. Plaskowski, M. S. Beck, R. Thron and T. Dyakowski, *Imaging Industrial Flows: Applications of Electrical Process Tomography*, IOP Publishing Ltd., U.K., 1995.

[10] T. T. Zin, H. Hama and P. Tin, Spatial image retrieval based on dynamic thresholding, *International Journal of Innovative Computing, Information and Control*, vol.5, no.11(B), pp.4051-4059, 2009.

[11] C. G. Xie, S. M. Huang, C. P. Lenn, A. L. Stott and M. S. Beck, Experimental evaluation of capacitance tomographic flow imaging systems using physical models, *IEE Proc. of Circuits Devices System*, pp.357-368, 1994.